Characterization, Crystallization Kinetics, and Melting Behavior of Poly(ethylene succinate) Copolyester Containing 7 mol % Butylene Succinate

Hsin-Ying Lu, Shih-Fu Lu, Ming Chen, Chi He Chen, Chia-Jung Tsai

Institute of Materials Science and Engineering, National Sun Yat-Sen University, Kaohsiung 80424, Taiwan, Republic of China

Received 1 June 2008; accepted 26 December 2008
DOI 10.1002/app.29975
Published online 30 March 2009 in Wiley InterScience (www.interscience.wiley.com).

ABSTRACT: The copolyester was synthesized and characterized as having 92.7 mol % ethylene succinate units and 7.3 mol % butylene succinate (BS) units in a random sequence, as determined by the use of nuclear magnetic resonance. Isothermal crystallization kinetics of this copolyester was examined in the temperature range (T_c) from 30 to 80°C with the use of differential scanning calorimetry (DSC). The melting behavior after isothermal crystallization was studied with DSC by varying the T_c, the heating rate, and the crystallization time. The complex melting behavior involves both mechanisms of various lamellar crystals and melting–recrystallization–remelting. As the T_c increases, the contribution of recrystallization gradually decreases and finally disappears. The Hoffman–Weeks linear plot yielded an equilibrium melting temperature of 111.1°C, which is 1.6°C less than that of poly(ethylene succinate) (PES). The kinetic analysis of the spherulitic growth rates (G) indicated that a regime II→III transition occurred at ~59°C ($T_{II\rightarrow III}$), which is ~ 11°C less than that of PES. The overall crystallization rate, $T_{II\rightarrow III}$ and G indicate that the random incorporation of only 7.3 mol % BS units into PES significantly inhibits the crystallization rate of PES. Finally, the morphology of melt-crystallized samples was examined using polarized light microscopy and scanning electron microscopy. © 2009 Wiley Periodicals, Inc. J Appl Polym Sci 113: 876–886, 2009

Key words: crystallization; morphology; polyesters

INTRODUCTION

Plastics have been used extensively in the last several decades because they are convenient and perform well. Environmental protection recently has become an important policy issue for every government. Pollution by chemosynthetic polymers has caused a global environmental problem because they are not degradable but stable. Biodegradable polymers are friendly to our ecosystem and provide alternative solutions for managing solid waste. Aliphatic polyesters are biodegradable because they are susceptible to enzymes and microorganisms. Two general methods exist for obtaining biodegradable polymers; they are biosynthesis and chemosynthesis. Poly(ethylene succinate) (PES) has a relatively high melting point (T_m, 103–106°C) and some favorable mechanical properties that are similar to those of such extensively used polymers as low density polyethylene (LDPE), poly(propylene),[1] and others.

Chemical composition, crystalline structure, and morphology dominate the biodegradation rate.[2] Numerous researchers have found that the degree of crystallinity, spherulite size, and lamellar structure can affect the biodegradation rate because biodegradation initially occurs in the amorphous region, such that the rate of erosion in the amorphous region substantially exceeds that in the crystalline region.[3,4] Therefore, research on the relationship among structure, crystallization kinetics, and morphology must precede research on degradation behavior, and the results thus obtained will help elucidate the degradation mechanism, supporting the design and development of various practical degradable polymers.

PES and poly(butylene succinate) (PBS) are promising candidate degradable aliphatic polyesters because they have favorable mechanical properties. The crystalline structure[5–8] and the crystal growth kinetics[2,9] of PES have been investigated. The dependence of the crystallization rate and the primary nucleation rate of PES on molecular weight also have been studied.[10,11] A few works of the multiple melting behaviors of PES have been published.[2,9,12–14] PBS exhibits a lower biodegradation than PES because it has a higher crystallization rate and

Correspondence to: M. Chen (mingchen@mail.nsysu.edu.tw).

Contract grant sponsor: National Science Council of the Republic of China, Taiwan; contract grant number: NSC 96-2221-E-110-045.

greater crystallinity. The crystalline structure of PBS has been investigated extensively.[15–17] The crystallization, spherulite morphology, and melting behavior of PBS also have been elucidated.[14,18–21] Approaches have been used to promote the physical properties or extend the range of application of PBS. They include physical blending, copolymerization, and formation of composite with organoclay. Copolymers are well known to have higher degradation rates than homopolymers, which is basically attributed to the limited crystallinity. In most copolymers in which both components are crystallizable, the degree of crystallinity declines as the proportion of the minor component increases because of incompatibility between the crystal lattices of both components.[22,23]

The aim of these works is to investigate the succinates that were synthesized by copolymerization of succinic acid with different diols (ethylene, 1,3-propylene, 1,4-butylene, etc.). PES, PBS, and a series of their random copolymers were recently synthesized in the laboratory.[24] The measurements of wide-angle X-ray diffraction (WAXD) patterns and heating thermograms indicate that the incorporation of minor amounts of butylene succinate (BS) units into PES significantly inhibits the crystallization behavior of PES. The glass transition temperature (T_g) decreases from -10.8 to -41.1°C as the BS content increases from 0 to 100%. A series of PES and PBS copolymers have been studied,[21,25,26] and a PBS-*co*-14%PES copolyester has been extensively reported.[20,27] To increase the biodegradation rate without sacrificing the melting temperature of PES, a copolymer with only 7 mol % BS, PES-*co*-7%PBS, was synthesized and characterized in this work. The differential scanning calorimetric (DSC) data were analyzed over a wide range of isothermal crystallization temperatures (T_c) by use of the Avrami equation.[28,29] Additionally, the origin of the multiple melting behaviors of isothermal crystallized specimens was elucidated with WAXD and DSC. The linear growth rates and the morphology of spherulites were obtained under a polarized light microscope (PLM), and the regime transition temperature was determined with the Lauritzene-Hoffman equation.[30] The surface texture of PES-*co*-7%PBS after hydrolysis was observed under a scanning electron microscope (SEM).

EXPERIMENTAL

Synthesis and characterization

Ethylene glycol (EG) (Showa, 99.5%), 1,4-butanediol (BD) (Acros, 99%), and succinic acid (SA) (Acros, 99%) were used without purification. Titanium tetraisopropoxide (TTP) (Acros, 98+%) was used as received. Other solvents used in the analysis were also used without further purification. The reaction mixture was charged into a 1-L stainless reactor with an EG : BD : SA molar ratio of 0.95 : 0.05 : 1. TTP was used as a catalyst: the amount was 0.1% of the amount of diacid used. PES-*co*-7%PBS copolyester was synthesized via a two-step esterification reaction in the melt. It was purified after it was dissolved in chloroform and precipitated into ten times as much vigorously stirred ice-cooled methanol. The precipitate was filtered, washed in methanol, and dried at reduced pressure and at room temperature. This copolyester had an intrinsic viscosity [η] of 1.25 dL/g, measured in phenol/1,1,2,2-tetrachloroethane (3/2, w/w) at 30°C. The number and weight average molecular weights, M_n and M_w, were 1.83×10^5 and 2.60×10^5 g/mol, respectively, relative to poly(methyl methacrylate). The T_g of an amorphous specimen was obtained using a Perkin-Elmer Pyris 1 DSC (Shelton, CT) at a heating rate of 10°C/min. The corresponding T_g was -11.7°C (261.4 K). The ^{13}C-NMR spectrum of *d*-chloroform solution was obtained with tetramethylsilane (TMS) as the reference standard using a Varian UNITY INOVA–500 NMR spectrometer (Palo Alto, CA) at 295.5 K.

All of the PES-*co*-7%PBS sheets were prepared in a hot press machine. These sheets were formed by compression molding for 5 min at 115°C. During the molding process, the mold was pressed and released several times to ensure void-free sheet. The sheet was then allowed to cool slowly to room temperature. The compressed sheet had a thickness of approximately 0.2 mm for use in DSC studies or about 0.5 mm for obtaining WAXD patterns. Both purified PES-*co*-7%PBS and sheets were dried at room temperature in a vacuum oven for 12 h to remove moisture before they were used.

DSC and specimen preparation

A Perkin–Elmer Pyris 1 DSC, equipped with a refrigerating system (Pyris Intracooler 2P), was calibrated with deionized water and indium. DSC was calibrated with the heat fusion of indium. A specimen with a weight 4 ± 0.5 mg was used. In the isothermal crystallization study, the samples were initially heated from 30 to 170°C at 20°C/min and then held at 170°C for 5 min. They were then rapidly cooled at a nominal rate of 250°C/min to a preset temperature (T_c) between 30 and 80°C and crystallized for a period that was three times the peak ending time, to ensure complete crystallization. After isothermal crystallization, the specimens were ready to be studied with DSC and SEM. The specimens were scanned up to 140°C at 10°C/min to elucidate their melting behavior. The samples were all treated under the same premelting conditions, except that the isothermal crystallization time was

varied, to study the sequence of the multiple melting peaks from the specimens that were crystallized at 62°C. They were then scanned directly from T_c up to 140°C at 10°C/min.

Specimens in TA sample pans were prepared isothermally in Pyris 1 DSC under the same conditions as described previously. A TA Instruments Q100 (New Castle, DE) equipped with a refrigerating system was used. The cell constant calibration was performed with an indium standard, and the temperature calibration was performed with deionized water and indium. To study the effect of the heating rate on the multiple melting peaks, the specimens crystallized at 62°C were scanned up to 136°C at 1, 10, 20, and 40°C/min, respectively, in conventional mode.

WAXD measurements

Specimens with a thickness of approximately 0.5 mm after complete isothermal crystallization at various T_c values were prepared using PLM under the same conditions as described in the section on DSC. X-ray diffractograms were obtained at room temperature using a Siemens D5000 diffractometer (Karlsruhe, Germany) and Ni-filtered Cu Kα radiation (λ = 0.1542 nm, 40 kV, 30 mA) at a scanning rate of 1°/min.

PLM measurements

A Nikon Optiphot-pol polarizing microscope (Tokyo, Japan) was employed in combination with a Linkam (Tadworth, UK) THMS–600 heating stage and a TMS–91 temperature control system. The video photograph system included a SONY DXC–755 CCD color video camera and a Pioneer DVR–510H DVD recorder. Measurements of spherulite growth rates were taken on a freshly made film, which was formed at temperatures between 100 and 105°C under nitrogen. The specimen was initially cooled, and then heated from room temperature at 20°C/min to 170°C, at which temperature it was maintained for 5 min to melt the crystalline residues. The premolten specimen was cooled rapidly to the required T_c, which ranged from 80 to 30°C. It was found that the homogeneous nucleation rate was very slow at temperatures above 60°C for PES[11] and PES dominated copolymer.[31] To save time, combining self-nucleation and nonisothermal temperature programs[32,33] were applied for $T_c \geq 60$°C. The premolten specimen was cooled down rapidly from 170 to 55°C, held for 15 min, and then heated at 50°C/min to T_c. The development of the spherulites was recorded as a function of time during crystallization. The growth rates of numerous spherulites in each specimen were examined.

SEM studies

Specimens, after complete isothermal crystallization at various T_c, were prepared under the same conditions as described in the section "DSC and specimen preparation." These specimens were immersed in 19 M sodium hydroxide solution at room temperature. The samples were removed from the solution after 4 h, washed in distilled water several times, and dried under a vacuum at room temperature. The etched surfaces of the samples were gold-coated and observed using a JEOL JSM–6400 SEM at an accelerating voltage of 15 kV.

RESULTS AND DISCUSSION

Copolyester composition and sequence distribution

Figure 1 displays the ^{13}C-NMR spectrum of the copolymer and the peak assignments. The two chemical shifts at 64.08–64.20 and 25.11–25.22 ppm are associated with the methylene carbons α and β bonded to the ester oxygen in the butylene group. The diol carbon atoms of ethylene group are at 62.25–62.38 ppm (C_2). The chemical shifts of the methylene group and the carbonyl group of succinic acid are at 28.70–29.00 (C_1) and 171.94–172.30 (C_5) ppm, respectively. A magnified view of the ^{13}C-NMR spectrum indicates that the signals of the carbonyl carbons (C_5) are split into three peaks, as presented in the inset in Figure 1. The assigned a–c peaks represent the carbonyl carbons of ESE, ESB-E side, and ESB-B side structures, respectively (where E represents EG unit, S is SA unit, and B denotes BD unit). This copolyester is characterized as having 92.7% ethylene succinate (ES) units and 7.3%

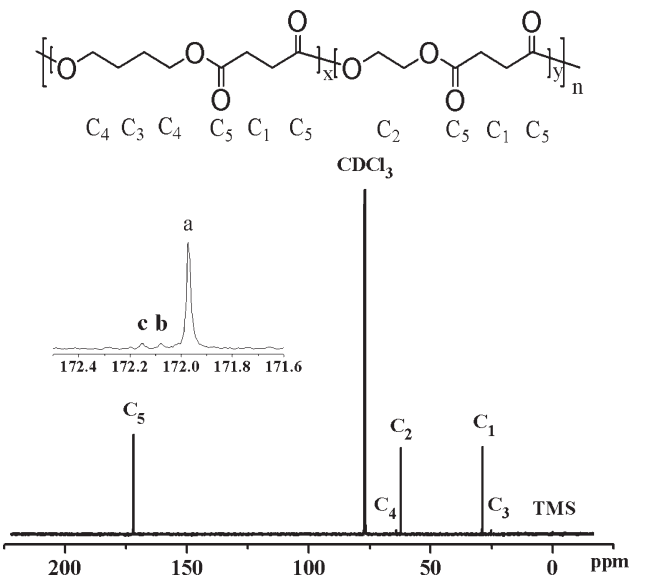

Figure 1 ^{13}C-NMR spectrum (solvent: *d*-chloroform at 295.5 K) and its peak assignments.

butylene succinate (BS) units, based on the analysis of carbonyl carbons. ES and BS units have average-number sequence lengths of 12.6 and 1.0, respectively. The randomness, B, is 1.08,[23,24] which is within the experimental error, $B = 1.0$ for a random copolyester. Therefore, the distribution of ES and BS units in this copolyester is supposed to be random given the presence of a single T_g at −11.7°C and a randomness value of 1.08.

WAXD results

Figure 2 presents WAXD patterns of this copolyester after crystallization at various isothermal temperatures and the WAXD pattern of PES that was isothermally crystallized at 80°C.[34] The crystal unit cell of PES is orthorhombic,[7,8] and the diffraction peaks from the (120) and (200) planes are observed at $2\theta \approx 20.2°$ and 23.4°, respectively. All the samples exhibit the same PES diffraction peaks over the entire range of temperatures, indicating only one crystalline form (α) in the samples that were crystallized isothermally between 30 and 80°C. As the T_c increases, these two diffraction peaks become sharper and the diffraction peak of the (121) plane turns out to be more pronounced, indicating improvement of crystalline order. The crystallinity increased from 27.5 to 30.7%, as determined from the relative areas under the crystalline peaks and the amorphous background. Accordingly, the multiple melting peaks may be associated with the melting of different populations of lamellar crystals and/or the melting of recrystallized crystals. PBS homopolymer has a monoclinic unit cell[15] and has a higher overall crystallization rate than PES. WAXD patterns and the average-number sequence length (1.0) show that a minor BS comonomer (unit) is excluded from PES crystals.[20]

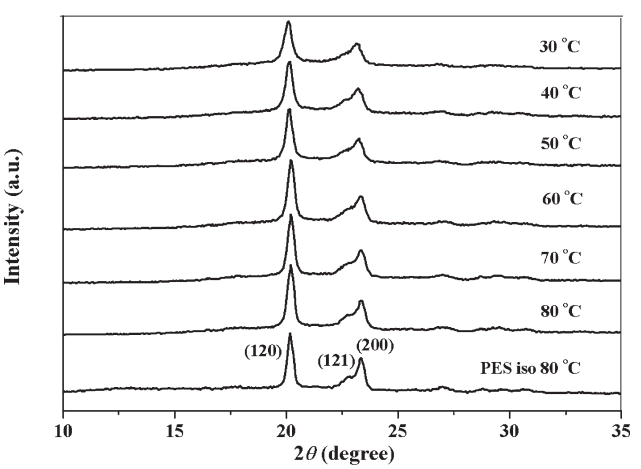

Figure 2 X-ray diffraction patterns of the PES-*co*-7%PBS specimens isothermally crystallized at various temperatures and of PES isothermally crystallized at 80°C.

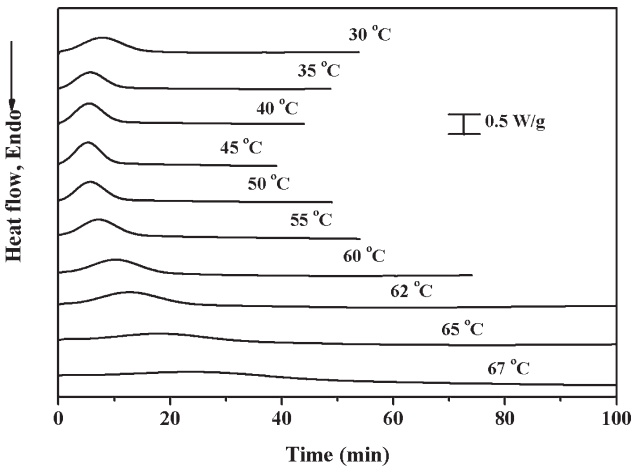

Figure 3 Crystallization isotherms of specimens at the indicated temperatures (T_c).

Isothermal crystallization kinetics

Figure 3 shows DSC exothermic traces of specimens that are isothermally crystallized at temperatures from 30 to 67°C. DSC traces are not presented for T_c greater than 67°C because the exothermic heat flow becomes too small and slow to be accurately defined the end of the crystallization process. The second column in Table I presents isothermal crystallization times (t_c) at temperatures from 30 to 80°C. The required t_c decreased from 55 min at 30°C to 40 min at 45°C, and then increased gradually to 300 min at 70°C, reaching 1000 min at 80°C. The exothermic trace was integrated to yield the heat of crystallization (ΔH_{exo}, third column), and the degree of crystallinity ($X_{c,exo}$) was determined by dividing the heat of crystallization by 163 J/g,[24] evaluated from the Flory equation. $X_{c,exo}$ increases from 26.2% at 35°C to 32.7% at 67°C, as indicated in column 4 of Table I. Because the isothermal crystallization at $T_c \geq 67$°C is slow, the values of ΔH_{exo} and $X_{c,exo}$ from 70 to 80°C were not estimated.

The relative degree of crystallinity at time t [$X_c(t)$] was calculated for each T_c. The half-time of crystallization ($t_{1/2}$ – defined as the time required for half of the final crystallinity to develop) was evaluated. The value of $t_{1/2}$ falls from 7.93 min at 30°C to 5.21 min at 45°C, and then increases gradually to 24.89 min at 67°C. Figure 4 plots the overall crystallization rate $(t_{1/2})^{-1}$ as a function of temperature as open squares. The curve reaches a maximum at approximately 45°C. For comparison, the $(t_{1/2})^{-1}$ values of PES[34] are also presented in Figure 4 using open triangle symbols. The maximum $(t_{1/2})^{-1}$ value of this copolyester is only half of that of PES.

It is well known that the Avrami equation[28,29] can be applied to describe the initial or the primary stage of isothermal crystallization of polymers, as followed:

TABLE I
Summary of the Condition and the Kinetic Analysis of Crystallization for the Isothermally Melt-Crystallized Specimens

T_c (°C)	t_c (min)	ΔH_{exo} (J/g)	$X_{c,exo}$ (%, abs)[a]	ΔH_{endo} (J/g)	$X_{c,endo}$ (%, abs)[a]	n_1	$X_c(t)$ range (%, rel)	r^2
30	55	−43.0	26.3	52.8	32.3	2.54	4.3–98.5	0.9996
35	50	−42.8	26.2	46.2	28.3	2.57	3.3–95.4	0.9998
40	45	−44.4	27.2	48.5	29.7	2.58	7.5–96.3	0.9998
45	40	−46.3	28.3	50.0	30.6	2.59	4.0–93.5	0.9996
50	50	−47.9	29.3	50.1	30.7	2.60	1.8–97.8	0.9997
55	55	−48.3	29.6	51.6	31.6	2.69	3.1–95.4	0.9998
60	75	−50.1	30.7	51.1	31.3	2.75	5.3–96.6	0.9995
62	110	−50.4	30.9	52.7	32.3	2.75	4.4–92.9	0.9995
65	180	−50.8	31.1	49.8	32.8	2.81	0.2–99.8	0.9998
67	250	−53.4	32.7	53.6	32.8	2.84	2.1–99.9	0.9995
70	300	–	–	50.8	32.9	–	–	–
75	500	–	–	54.4	33.3	–	–	–
80	1000	–	–	(54.3)	(33.2)	–	–	–

[a] Enthalpy of fusion of PES is 163 J/g.[24]

$$1 - X_c(t) = \exp(-k_1 t^{n_1}) \quad (1)$$

$$\log[-\ln(1 - X_c(t))] = n_1 \log t + \log k_1 \quad (2)$$

where k_1 is the crystallization rate constant and n_1 is the Avrami exponent describing the crystal geometry and nucleation mechanism. According to Equation (2), the plot of $\log[-\ln(1 - X_c(t))]$ versus $\log t$ will give the slope n_1 and the intercept $\log k_1$.

Figure 5 displays a typical Avrami plot for the specimen that was crystallized isothermally at 62°C. The best linear regression was obtained between the relative crystallinities of 4.4 and 92.9% with a correlation coefficient (r^2) of 0.9995, which values are listed in the T_c = 62°C row in Table I. This curve has an initial linear portion that corresponds to an Avrami exponent (n_1) of 2.75. The second linear part is fitted to the part that levels off. The point of intersection between these two linear regression lines was at 21.25 min, as shown in Figure 5. The Avrami plots yield n_1 and the rate constant (k_1) at various T_c values. As T_c increases, n_1 increases from 2.54 to 2.84, as shown in column 7 in Table I. k_1 increases first from 3.55×10^{-3} to 9.35×10^{-3}, and then declines to 7.53×10^{-5}; the results are plotted as filled circles in Figure 4. The k_1 values of PES[34] are displayed as filled triangles in the same figure for the comparison.

Figure 4 presents both the maximum values of $(t_{1/2})^{-1}$ and k_1 at 45°C. The maximum rate of spherulite growth (G) was at 52°C (described later). Umemoto et al.[11] measured the primary nucleation rate of PES. A maximum was found at 18–32°C, depending on the molecular weight. The nucleation rate of PES-*co*-7%PBS is less than that of PES, because incorporating BS units into PES markedly inhibits the crystallization behavior of PES. Therefore, the overall crystallization rate $(t_{1/2})^{-1}$ is maximal at a temperature between the temperatures of the maximum nucleation rate and the maximum growth rate.

The exponent n_1 decreases from 2.84 to 2.54 as T_c decreases. It is less than 4.0, which is the theoretical value in the case of sporadic nucleation and three-

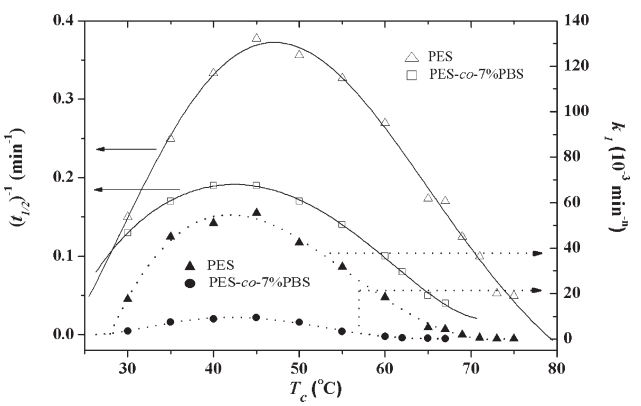

Figure 4 Temperature dependencies (T_c) of the overall crystallization rate $(t_{1/2})^{-1}$ and the rate constant (k_1).

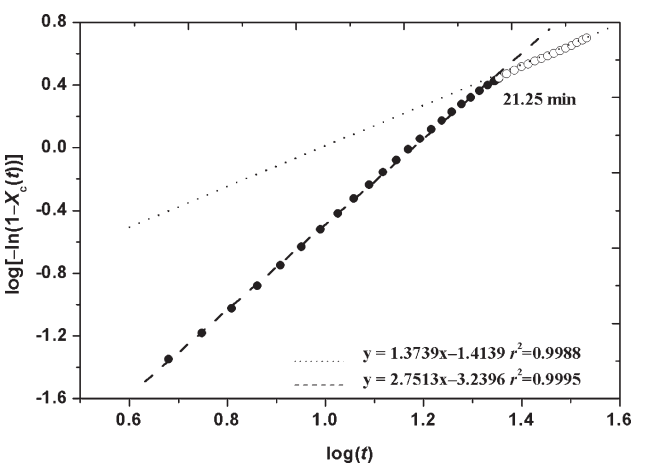

Figure 5 Plot of $\log[-\ln(1-X_c(t))]$ vs. $\log t$ for the specimens crystallized isothermally at 62°C.

dimensional crystal growth, for the following reasons. First, the thickness of the samples for the DSC studies is approximately 0.2 mm. At higher T_c values, the nucleation density is low and the diameter of the spherulite is about 0.1 mm. Therefore, the growth of the spherulites was restricted to two dimensions during the latter stage of isothermal crystallization. Second, the growth rate of this copolyester is low, reaching a maximum value of 6.58×10^{-2} μm/s (described later). The primary and secondary crystallizations are suggested to proceed simultaneously before the impingement of crystals. (See Table I and the following paragraph) Third, the homogeneous nucleation rate increases as T_c declines, representing an athermal nucleation process that is followed by three-dimensional crystal growth during the early stage of isothermal crystallization. Finally, the cooling rate of the refrigerating system is not sufficiently high to prevent crystallization of this copolyester before it is cooled to a low T_c. Similar results have been observed in an earlier study for PES copolyester that contains 5 mol % trimethylene succinate.[31,34]

Melting behavior of specimens crystallized at 62°C

The premelting temperature of isothermal crystallization was maintained for 5 min at 170°C, which was 59°C higher than T_m^0 (111.1°C, Fig. 9). Following this premelting treatment, the subsequent isothermal crystallization behavior was independent of the prior thermal history. The maximum growth rate of spherulite was 6.58×10^{-2} μm/s at 52°C. The growth rate was 4.88×10^{-2} μm/s at 62°C. PLM experiments indicated that the homogeneous nucleation rate of

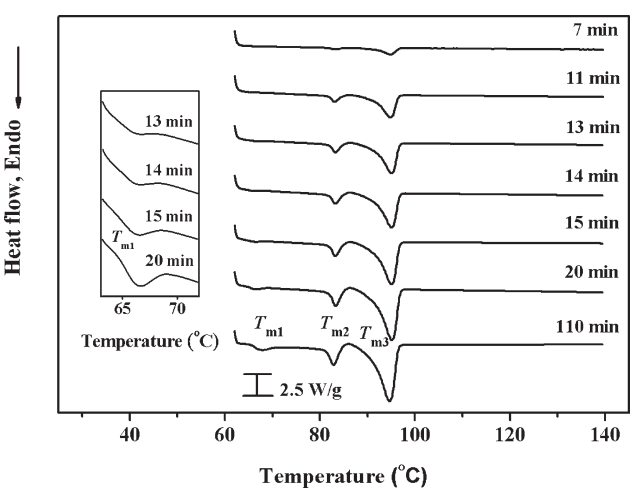

Figure 6 DSC thermograms (at a heating rate of 10°C/min) for specimens after premelting at 170°C for 5 min, and then crystallized isothermally at 62°C for periods of time.

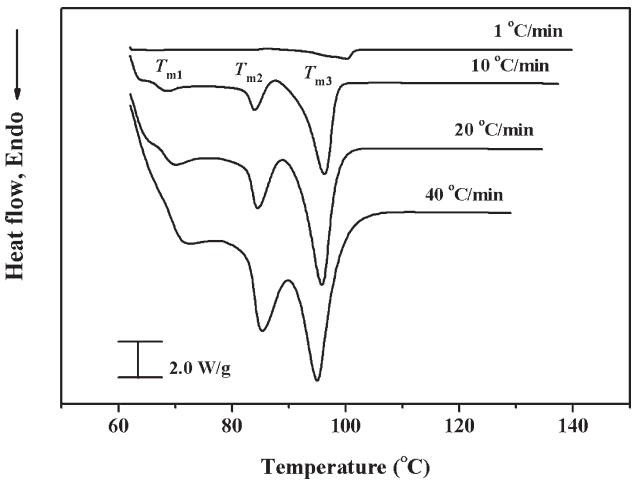

Figure 7 DSC thermograms at different heating rates for specimens crystallized isothermally at 62°C. These measurements were made on a Q100 instrument in conventional mode.

PES-*co*-7%PBS was very low at temperatures of over 60°C,[11,31] and that the regime II → III transition occurred at approximately 59°C. In general, the crystals that formed in regime III had more defects and lower crystallinity than those that formed in the other regimes. These results are used to elucidate the melting behavior following complete isothermal crystallization at 62°C.

Figure 6 displays DSC thermograms obtained at a heating rate of 10°C/min for specimens that had been isothermally crystallized at 62°C. The inserts in the left-hand side of this figure enlarge the thermograms at around 67°C. Specimens crystallized isothermally for 11 or ≥13 min, yield double or triple melting peaks, respectively. The peak temperatures of the melting peaks are denoted T_{m1}, T_{m2}, and T_{m3} in order of increasing temperature (as in both Figs. 7 and 8). Small amount of exothermically produced heat can be found between the two upper melting peaks, and the enthalpy of the exotherm increases slightly with the crystallization time. However, this exothermic curve is much lower than the peak at T_{m3}, because both the nucleation rate and the crystal growth rate are low (or the recrystallization rate is low) at 62°C. Therefore, the ratio of intensity of the peak at T_{m3} to that at T_{m2} varies very little. These results indicate that the upper peaks at T_{m2} and T_{m3} appear initially and the lower peak at T_{m1} appears after further crystallization. The minimum time for the occurrence of T_{m1} (∼ 13 min) is less than 21.25 min (Fig. 5). As presented in the final two columns of Table I, the range of relative crystallinities (4.4–92.9%) in which the curve is initially linear also suggests that the endothermic peak at T_{m1} (the secondary process) arises before the spherulites have impinged on each other.

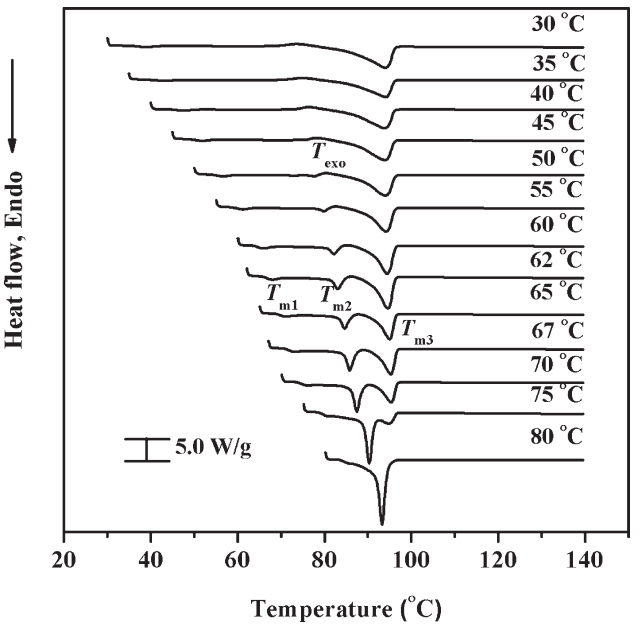

Figure 8 DSC thermograms (at a heating rate of 10°C/min) for specimens isothermally melt-crystallized at the indicated temperatures.

Figure 7 presents DSC thermograms obtained at four heating rates for specimens after complete isothermal crystallization at 62°C. When the heating rate is increased from 1, 10, 20, to 40°C/min, triple melting peaks are observed as follows. The peaks at T_{m1} (~ 69°C) and T_{m2} (~ 85°C) shift to a greater temperature and increase in intensity. The exothermic peak just before the major melting peak (T_{m3}) slowly decreases to zero. The peak at T_{m3} (about 97°C) shifts to a lower temperature but its intensity increases with the heating rate. The ratio of the intensities of the upper two melting peaks declines significantly as the heating rate increases, because less time is available for the recrystallization and/or reorganization during the heating scan. As the heating rate increases from 1 to 10°C/min, the enthalpy of the recrystallization becomes lower, such that the contribution of remelting to the main melting peak becomes less. The remelting peak is distinct in the case of PES with a viscosity molecular weight of 10,000.[12,13] The molecular weight of PES[24] synthesized in the authors' laboratory is higher than that of any PES used in the cited papers.[2,9,12–14] The maximum growth rate in one such investigation[24] is only half of that in another.[2] As stated previously, incorporating BS units into PES significantly inhibits the crystallization behavior of PES. The spherulitic growth rate and recrystallization rate of this PES-*co*-7%PBS are expected to be lower than those of PES. Therefore, the peaks at T_{m2} and T_{m3} in Figures 6 and 7 are due primarily to the melting of different populations of lamellar crystals.

Elucidating the melting behavior

Figure 8 presents the results of DSC heating scans at a heating rate of 10°C/min. The heating curves exhibit multiple endothermic peaks. A small exothermic peak is detected just before the melting of peak at T_{m3}, and is denoted as T_{exo}. T_{m1} is 5–10°C above T_c. The peak at T_{m2} appears when $T_c \geq 50$°C and becomes a major peak for $T_c \geq 75$°C. The peaks at T_{m1} and T_{m2} shift to higher temperatures and increase in intensity as T_c increases. This trend demonstrates that thicker crystalline lamellae develop as T_c increases. The position and intensity of the peak at T_{m3} vary very little with T_c, but the area under the peak declines as T_c increases from 30 to 70°C. The ratio of intensity of the peak at T_{m3} to that at T_{m2} increases significantly as T_c decreases, because the melting temperature of the secondary crystals (T_{m1}) decreases, and more time is allowed to recrystallize during the heating scan. These results reveal that the lower-temperature part of the peak at T_{m3} is related to the melting of the recrystallized crystals.[31] As T_c increases, the contribution of the melting–recrystallization–remelting process to the upper melting peak slowly declines and finally disappears. Therefore, the peak at T_{m2} is attributed to the fusion of the crystals that grow during primary crystallization. The origin of the peak at T_{m1} is still under debate. Interpretation includes the superposition of melting and recrystallization,[9,35–37] the enthalpic relaxation of the rigid amorphous fraction,[38,39] and both of these two mechanisms.[40] Some progresses are caused by new techniques; however, different polymers have different characteristics. The growth rates of crystals should be correlated with the overall crystallization rate and the melting behavior obtained from DSC. In the study of two copolyester series of poly(trimethylene terephthalate-*co*-ethylene terephthalate)[41–44] and poly(ethylene succinate-*co*-trimethylene succinate),[23,31,45] it was found that the peak at T_{m1} turns out to be more pronounced when the amount of the minor comonomer increases because both the growth rate and overall crystallization rate of the copolyester decreases. Therefore, the peak at T_{m1} is primarily associated with the melting of the secondary crystals in this study. Furthermore, the melting temperature is rigorously defined as the temperature at which the last trace of crystals melts, and is given by $T_{m3\text{-end}}$. $T_{m3\text{-end}}$ remains constant at 94.5 ± 0.5°C. The fifth column of Table I presents the measured total enthalpy of melting (ΔH_{endo}). Its value increases from 46.2 to 54.4 J/g as T_c increases from 35 to 75°C. The corresponding degree of crystallinity ($X_{c,endo}$) increases from 28.3 to 33.3%, as indicated in the sixth column of Table I.

Figure 9 plots T_{m1} and T_{m2} as functions of T_c. A solid line is drawn where $T_m = T_c$. The values of

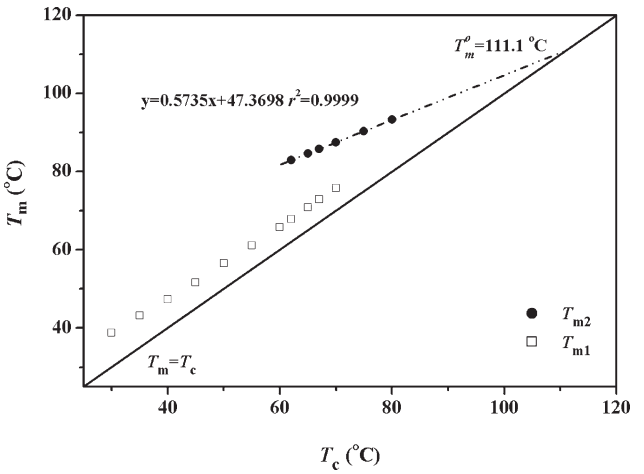

Figure 9 Hoffman–Weeks plot for determining the equilibrium melting temperature of the copolyester from DSC data at a heating rate of 10°C/min.

T_{m1} (open squares) fall on a line with a slope of 0.9142, approaching the $T_m = T_c$ line as T_c increases. According to the Hoffman–Weeks approach,[46] the values of T_{m2} are extrapolated (based on a linear regression of the filled circular points with T_cs = 62, 65, 67, 70, 75, and 80°C) until they intersect with the solid line. The temperature of the intersection is T_m^0, which equals 111.1°C. This value is approximately 16.5°C greater than $T_{m3\text{-end}}$. This T_m^0 that is estimated from the Hoffman–Weeks plot may be less reliable, but the regime transition temperature $T_{II\rightarrow III}$ can be assumed to be almost independent of the values of T_m^0.[20]

Kinetic analysis of growth rates of spherulites

The growth rate (G) of spherulites was determined before their impingement by measuring the spherulitic radii from PLM micrographs taken at intervals during the isothermal crystallization. Figure 10 plots the temperature-dependence of the growth rate as open circles. The growth rate increases smoothly from 2.11 $\times$ 10^{-2} μm/s at 30°C, passing a maximum of 6.58 $\times$ 10^{-2} μm/s at 52°C, before falling smoothly to 0.46 $\times$ 10^{-2} μm/s at 80°C. Figure 10 also plots the growth rates of PES[31,34,45] as open squares. The maximum growth rate of this PES-*co*-7%PBS copolyester is about half of that of PES. One of the reasons for this result is that incorporating BS units into PES significantly inhibits the crystallization of PES.

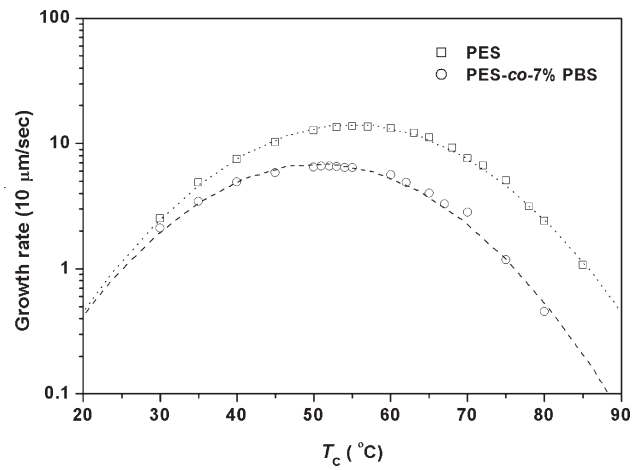

Figure 10 Variation of spherulitic growth rates with temperature.

According to the secondary nucleation theory of Lauritzen–Hoffman (LH),[30] the spherulitic growth rates can be expressed as

$$G = G_0 \exp\left[\frac{-U^*}{R(T_c - T_\infty)}\right] \exp\left[\frac{-K_g}{T_c(\Delta T)f}\right] \qquad (3)$$

where G_0 is a preexponential factor, R represents the gas constant, U^* is the activation energy of reptational diffusion, T_∞ is a hypothetical temperature below which motion ceases, $\Delta T = (T_m^0 - T_c)$ represents undercooling, and f is a correction term of the order of unity, and is usually given by $f = 2T_c/(T_m^0 + T_c)$. The regime analysis based on the LH model is applied to the growth rate data that are plotted in Figure 10. Figure 11 plots $\log G + U^*/[2.303R(T_c - T_\infty)]$ as a function of $1/(T_c\Delta Tf)$, yielding K_g (slope $\times$ 2.303) in each regime. The regime analysis of the LH model was performed using the following values; U^* = 5,950 cal/mol and $T_\infty = T_g - 30$ K with T_g at 261.4 K. T_m^0 = 111.1°C = 384.2 K was adopted. The two optimal fit lines correspond to the correlation coefficients (0.9955 and 0.9958), as plotted in Figure 11. The curve is broken at T_c = 59.2°C and the ratio of the two slopes is 2.00.

Columns 3 to 8 in Table II present the calculated values of K_g, correlation coefficient (r^2) and $T_{II\rightarrow III}$

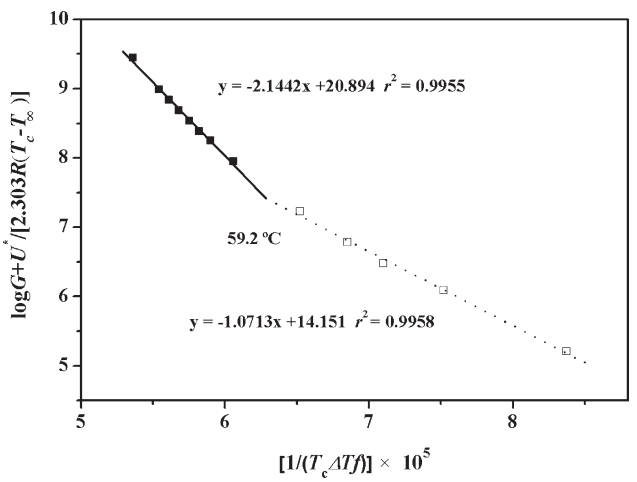

Figure 11 Kinetic analysis of the growth rate data of spherulites. In this case, U^* = 5,950 cal/mol, and $T_\infty = T_g$ - 30 K.

TABLE II
Values of K_g, Correlation Coefficient, and Transition Temperature Determined from Secondary Nucleation Theory

T_∞ (K)	U^* (cal/mol)	K_g(III) $\times 10^{-5}$	r^2(III)	K_g(II) $\times 10^{-5}$	r^2(II)	K_g(III)/K_g(II)	$T_{II\rightarrow III}$ (°C)
T_g-30	1,500	–	–	–	–	–	–
T_g-30	5,950	4.94	0.9955	2.47	0.9958	2.00	59.2
T_g-51.6	4,200	2.33	0.9992	1.60	0.9973	1.45	59.4
T_g-51.6	10,400	5.69	0.9958	2.85	0.9954	2.00	59.3

(transition temperature of regime II→III) as T_∞ and U^* were varied. In the first and second rows for which T_∞ is T_g – 30 K, $T_{II\rightarrow III}$ is not obtained when U^* is 1500 cal/mol. For $T_\infty = T_g$ – 51.6 K, the ratio of K_g(III)/K_g(II) increases from 1.45 to 2.00 as U^* is changed from 4200 to 10,400 cal/mol. The respective values of $T_{II\rightarrow III}$ are 59.4 and 59.3°C (rows 3 and 4). These results have indicated that PES-*co*-7%PBS exhibits a regime II→III transition at 59.3 ± 0.1°C, which is approximately 11°C less than that of PES.[31,45]

Morphology of spherulites

Figure 12 presents the samples, crystallized from the melt at various T_c, between the crossed polarizing

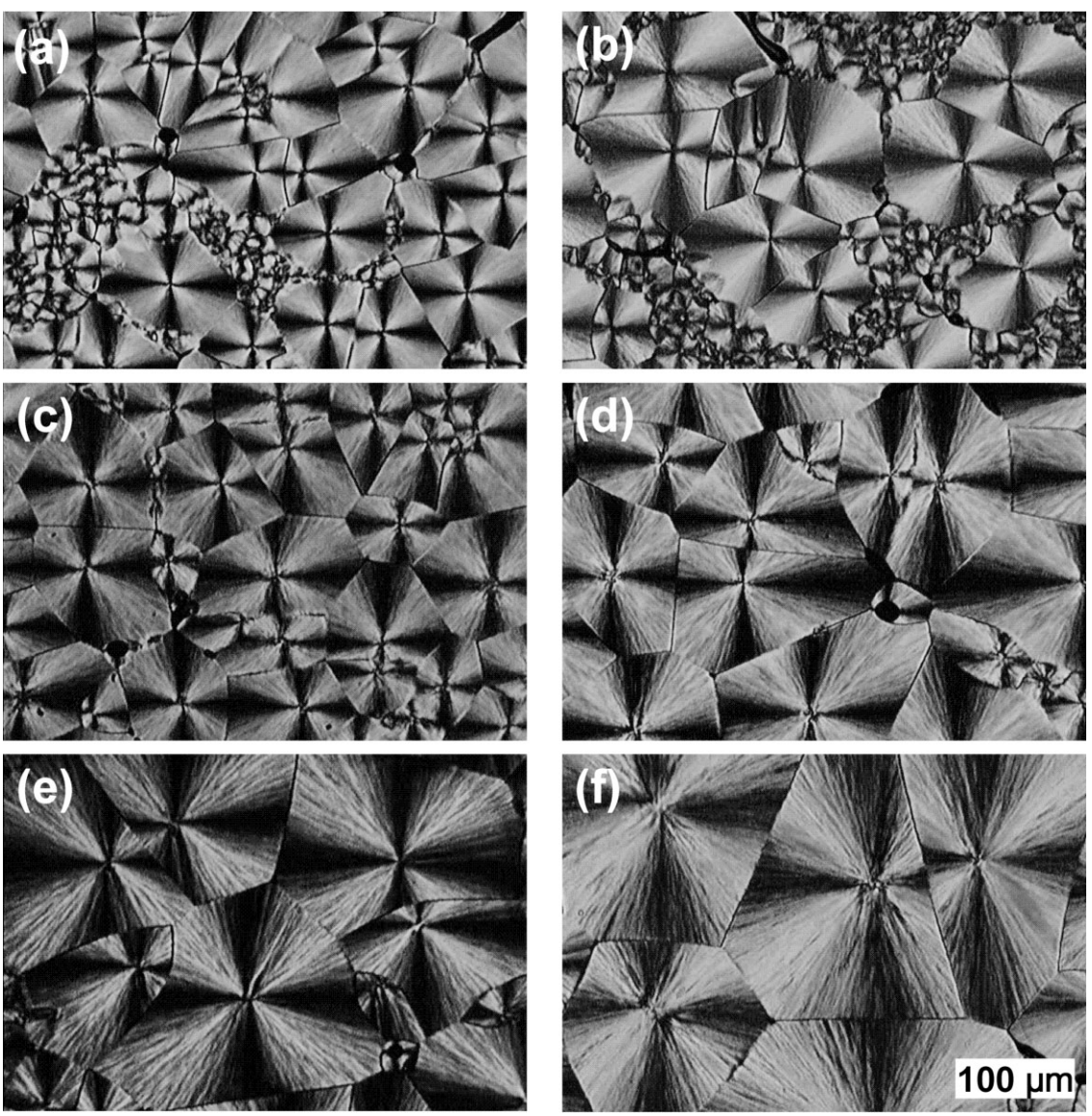

Figure 12 Representative PLM micrographs for specimens melt-crystallized at the indicated temperatures: (a) 50, (b) 55, (c) 57, (d) 60, (e) 62, and (f) 65°C. The scale bar of 100 μm at the lower right applied to all six micrographs.

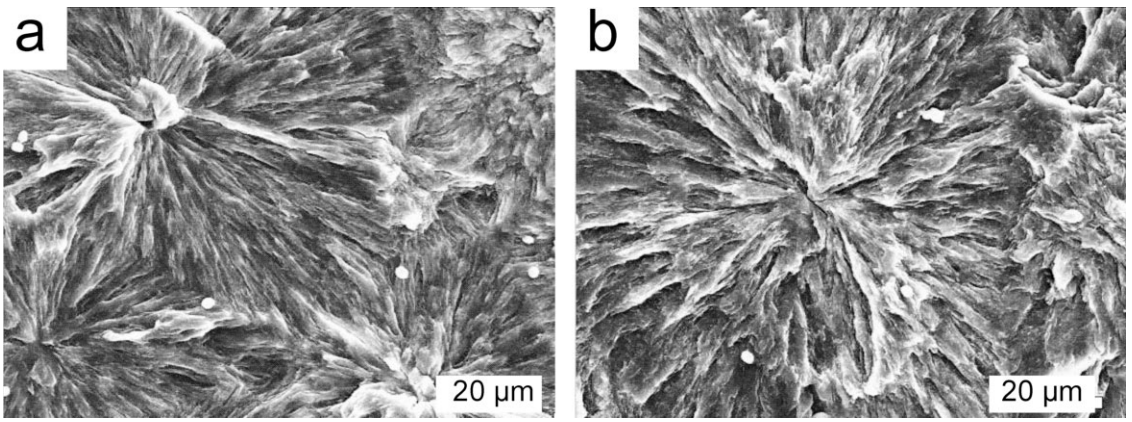

Figure 13 SEM images after etching for specimens melt-crystallized at the indicated temperatures: (a) 60 and (b) 70°C.

plates. The optical behavior of these spherulites exhibited typical negative birefringence, marked by a dark Maltese cross. Morphology did not change abruptly as T_c was increased from 30 to 55°C. Figure 12 (a) and (b) show small crystals in clusters because the homogeneous nucleation rate increases rapidly as T_c is in regime III. The number of spherulites decreases as T_c increases from 57 to 65°C, as displayed in Figure 12(c–f). Because self-nucleation method was applied for the experiments of $T_c \geq$ 60°C, straight boundaries can be found in Figure 12(d–f). Gan et al.[2] indicated that the radiating lines from the center of the PES spherulites became coarse as T_c increases. They examined the morphological changes at the spherulitic level and lamellar level in regimes II and III using a PLM and atomic force microscope, indicating the presence of a transition from regime II to regime III at about 71°C. The incorporation of BS units into PES significantly inhibits the crystallization behavior of PES. The $T_{II\text{-}III}$ decreases from 71°C for PES to 59°C for PES-*co*-7%PBS. The increase in the coarseness of the PES-*co*-7%PBS spherulites can be assumed to be nearly 60°C, as revealed by the textures of Figure 12.

Figure 13 presents the SEM micrographs of etched PES-*co*-7%PBS samples that were isothermally crystallized at 60 and 70°C. The texture after hydrolysis reflects the size and shape of the lamella, which are composed of spherulites. These SEM observations of spherulite morphology are highly consistent with the PLM observations. These micrographs reveal that the hydrolysis preferentially attacked amorphous regions rather than crystalline regions.

CONCLUSIONS

This PES-*co*-7%PBS copolyester has 92.7 mol % ES units and 7.3 mol % BS units. The value of the random parameter, 1.08, is close to 1.0 for a random copolymer. The average-number sequence lengths of ES and BS units are 12.6 and 1.0, respectively. A single T_g also suggests that this copolymer is a random copolyester. Isothermal crystallization was associated with a drop in the n_1 values of the Avrami exponent from 2.84 to 2.54 as T_c decreased from 67 to 30°C. At higher T_c, the n_1 values of the Avrami exponent are less than the theoretical value of four because the secondary crystals may already grow within the primary crystal lamellae. The rate of overall crystallization is expected to be maximal at a temperature (45°C) between the temperature of the maximum nucleation rate and the temperature of the maximum growth rate (52°C). The growth rate data are examined using Hoffman–Lauritzen nucleation theory. The classical regime II→ III transition occurs at approximately 59.3°C.

WAXD patterns indicate that only one crystal structure formed isothermally between 30 and 80°C. DSC curves revealed triple melting peaks. The melting behavior was such that the upper two melting peaks appeared initially and then the lower melting peak occurred at a longer crystallization time. Weakly exothermic behavior between the upper two melting peaks provides direct evidence of recrystallization. As T_c increases, the contribution of recrystallization gradually declines and finally disappears. The absence of exothermic flow and the appearance of triple melting peaks support the involvement of various lamellar crystals. The linear Hoffman–Weeks plot yielded an equilibrium melting temperature of 111.1°C, which is 16.6°C greater than the melting temperature of the last trace of crystals. The copolymerization effect by feeding 5 mol % 1,4-butanediol on the melting temperature and crystallinity of PES can be found in this and previous studies. The effect of copolymerization on the biodegradability is still under investigation.

References

1. Tezuka, Y.; Ishii, N.; Kasuya, K.; Mitomo, H. Polym Degrad Stab 2004, 84, 115.

2. Gan, Z. H.; Abe, H.; Doi, Y. Biomacromolecules 2000, 1, 704.
3. Kumagai, Y.; Kanesawa, Y.; Doi, Y. Makromol Chem 1992, 193, 53.
4. Abe, H.; Doi, Y.; Aoki, H.; Akehata, T. Macromolecules 1998, 31, 1791.
5. Fuller, C. S.; Erickson, C. L. J Am Chem Soc 1937, 59, 344.
6. Bunn, C. W. Proc R Soc London 1942, A180, 67.
7. Ueda, A. S.; Chatani, Y.; Tadokoro, H. Polym J 1971, 2, 387.
8. Ichikawa, Y.; Washiyama, J.; Moteki, Y.; Noguchi, K.; Okuyama, K. Polym J 1995, 27, 1264.
9. Papageorgiou, G. Z.; Bikiaris, D. N. Polymer 2005, 46, 12081.
10. Takayangi, M. J Polym Sci 1955, 19, 200.
11. Umemoto, S.; Hayashi, R.; Kawano, R.; Kikutani, T.; Okui, N. J Macromol Sci Phys 2003, B42, 421.
12. Al-Raheil, I. A.; Qudah, A. M. A. Polym Int 1995, 37, 249.
13. Caminiti, R.; Isopo, A.; Orru, M. A.; Albertini, V. R. Chem Mater 2000, 12, 369.
14. Qiu, Z. B.; Komura, M.; Ikehara, T.; Nishi, T. Polymer 2003, 44, 7781.
15. Chatani, Y.; Hasegawa, R.; Tadokoro, H. Polym Prepr Jpn 1971, 20, 420.
16. Ihn, K. J.; Yoo, E. S.; Im, S. S. Macromolecules 1995, 28, 2460.
17. Ichikawa, Y.; Suzski, J.; Washiyama, J.; Moeki, Y.; Noguchi, K.; Okuyama, K. Polym J 1995, 27, 1230.
18. Miyata, T.; Masuko, T. Polymer 1998, 39, 1399.
19. Wang, X. H.; Zhou, J. J.; Li, L. Eur Polym J 2007, 43, 3163.
20. Gan, Z. H.; Abe, H.; Kurokawa, H.; Doi, Y. Biomacromolecules 2001, 2, 605.
21. Cao, A.; Okamura, T.; Nakayama, K. Polym Degrad Stab 2002, 78, 107.
22. Papageorgiou, G. Z.; Bikiaris, D. N. Biomacromolecules 2007, 8, 2437.
23. Tsai, C. J.; Chang, W. C.; Chen, C. H.; Lu, H. Y.; Chen, M. Eur Polym J 2008, 44, 2339.
24. Chen, C. H.; Lu, H. Y.; Chen, M.; Peng, J. S.; Tsai, C. J.; Yang, C. S. J Appl Polym Sci 2009, 111, 1433.
25. Mochizuki, M.; Mukai, K.; Yamada, K.; Ichise, N.; Murase, S.; Iwaya, Y. Macromolecules 1997, 30, 7403.
26. Yoo, Y. T.; Ko, M. S.; Han, S. B.; Kim, T. Y.; Im, S. S.; Kim, D. K. Polym J 1998, 30, 538.
27. Gan, Z. H.; Abe, H.; Doi, Y. Biomacromolecules 2001, 2, 313.
28. Avrami, M. J Chem Phys 1939, 8, 212.
29. Avrami, M. J Chem Phys 1941, 9, 177.
30. Hoffman, J. D.; Davis, G. T.; Lauritzen, J. I., Jr. Treatise on Solid State Chemistry; Plenum Press: New York, 1976; Vol. 3, Chapter 7.
31. Chen, M.; Chang, W. C.; Lu, H. Y.; Chen, C. H.; Peng, J. S.; Tsai, C. J. Polymer 2007, 48, 5408.
32. Chen, M.; Chung, C. T. J Polym Sci Part B: Polym Phys 1998, 36, 2393.
33. Di Lorenzo, M. L.; Cimmino, S.; Silvestre, C. Macromolecules 2000, 33, 3828.
34. Chang, W. C. Master Thesis, National Sun Yat-Sen University, Kaohsiung, Taiwan, 2006 (in Chinese).
35. Minakov, A. A.; Mordvintsen, D. A.; Tol, R.; Schick, C. Thermochim Acta 2006, 442, 25.
36. Wei, C. L.; Chen, M.; Yu, F. E. Polymer 2003, 44, 8185.
37. Sauer, B. B.; Kampert, W. G.; Neal Blanchard, E.; Threefoot, S. A.; Hsiao, B. S. Polymer 2000, 41, 1099.
38. Lu, S. X.; Cebe, P. Polymer 1996, 37, 4857.
39. Cheng, S. Z. D.; Wunderlich, B. Macromolecules 1988, 21, 789.
40. Righetti, M. C.; Di Lorenzo, M. L.; Tombari, E.; Angiuli, M. J Phys Chem B 2008, 112, 4233.
41. Ko, C. Y.; Chen, M.; Wang, H. C.; Tseng, I. M. Polymer 2005, 46, 8752.
42. Ko, C. Y.; Chen, M.; Wang, C. L.; Wang, H. C.; Chen, R. Y.; Tseng, I. M. Polymer 2007, 48, 2415.
43. Chen, M.; Ko, C. Y.; Wang, H. C.; Chen, R. Y.; Wang, C. L.; Lu, H. Y.; Tseng, I. M. J Appl Polym Sci 2009, 112, 2305.
44. Chen, M.; Wang, H. C.; Ko, C. Y.; Chen, R. Y.; Wang, C. L.; Tseng, I. M. Polym Int 2008, 57, 297.
45. Lu, H. Y.; Peng, J. S.; Chen, M.; Chang, W. C.; Chen, C. H.; Tsai, C. J. Eur Polym J 2007, 43, 2630.
46. Hoffman, J. D.; Weeks, J. J. J Res Natl Bur Stand 1962, 66A, 13.